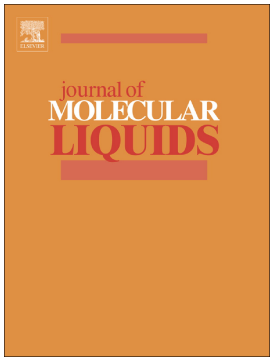

Synthesis and structural characterization of some divalent metal complexes: DNA binding and antitumor activity

A.A. El-Bindary, N. Hassan, M.A. El-Afify

PII: S0167-7322(17)32177-3
DOI: doi: 10.1016/j.molliq.2017.07.009
Reference: MOLLIQ 7586

To appear in: *Journal of Molecular Liquids*

Received date: 17 May 2017
Revised date: 2 July 2017
Accepted date: 4 July 2017

Please cite this article as: A.A. El-Bindary, N. Hassan, M.A. El-Afify , Synthesis and structural characterization of some divalent metal complexes: DNA binding and antitumor activity, *Journal of Molecular Liquids* (2017), doi: 10.1016/j.molliq.2017.07.009

Synthesis and structural characterization of some divalent metal complexes: DNA binding and antitumor activity

A.A. El-Bindary[1,*], N. Hassan[2], M.A. El-Afify[2]

[1]Chemistry Department, Faculty of Science, University of Damietta, Damietta 34517, Egypt

[2]Chemistry Department, Faculty of Science, University of Port Said, Egypt

[*]Corresponding author. **E-mail: abindary@yahoo.com** (A.A. El-Bindary).

Abstract

New Complexes (1-4) of Cu(II), Ni(II) Zn(II) and Mn(II) with 3-Ethoxy-6-(phenyl azo)-7-hydroxy coumarin (HL) have been prepared and characterized by elemental analyses, IR, ^{1}H NMR, ^{13}C NMR, mass spectroscopy and UV–Visible spectra as well as thermal measurements. IR spectra showed that the ligand (HL) acts as a monobasic bidentate and coordinating via the nitrogen atom of the azo group (-N=N-) and oxygen atom of the deprotonated phenolic OH group. The molar conductance measurements proved that all the complexes are non-electrolytes. Also the important fragments in the ligand and Ni(II) complex were done using mass spectra and the main peaks were corresponding to the molecular weights. The molecular and electronic structures of the investigated compounds were also studied using quantum chemical calculations. The bonding parameter of the complexes have been calculated. Molecular docking was used to predict the binding between azo compound with the receptor of 3hb5-oxidoreductase receptor of breast cancer and of 2q7k-hormone of prostate cancer. The calf thymus DNA binding activity of the ligand and its metal complexes was studied by absorption spectra and viscosity measurement. The antitumor activity of the ligand and its metal complexes was tested against human cancer MCV-7 (breast cancer).

Keywords: Azo coumarin**;** Molecular structure; Molecular docking**;** CT-DNA binding; Antitumor.

1. INTRODUCTION

Coumarin (2H-1-benzopyran-2-one), the parent molecule of coumarin derivatives, is the simplest compound of a large class of naturally occurring phenolic substances made of fused benzene and a-pyrone rings [1]. Coumarins owe their class name to 'Coumarou', the vernacular name of the tonka bean (Dipteryx odorata Willd, Fabaceae), from which coumarin, it was isolated in 1820 (Bruneton, 1999). There are four main coumarin sub-types: Coumarin and its derivatives are principal oral anticoagulants. Coumarin is water insoluble; however 4-hydroxy substitution confers weakly acidic properties to the molecule that makes it water soluble under slightly alkaline conditions.

Many products which contain a coumarin moiety exhibit excellent biological activity such as molluscicides, anthelmintic, hypnotic, insecticidal, activity fluorescent brighteners, antitumor [2], antibacterial [3], antifungal [4], anticoagulant [5], estrogenic, vasodilator, sedative, analgesic and hypothermic activity and anti-inflammatory [6]. In addition, these compounds are used as additives to food and cosmetics preparation as a dye and preservatives [7]. As like coumarin, azo dye functional group containing compound are have huge important is there commercially, it act as anti-microbial, and food coloring agent [8]. We felt it of interest to study the chemical reactivity of these heterocyclic coumarin moieties fuse with azo dyes to give a novel azo coumarin dye obtained by the diazotization followed by coupling with aromatic hydro carbon. The synthesized compound influencing biological behaviors of individual coumarin as well as azo dye compound. Monohydroxy compounds containing coumarin nucleus have proved to be of great importance, introduction of azo group to such hydroxy coumarins increases its chelating tendency. The formation of diazotizing reagent starts with protonation of nitrous acid under strongly acidic conditions and azo coupling is carried out at low temperature in the presence of nucleophilic coupling components. They exist in the trans form with a bond angle of 120˚ [9]. The complexes of azo compounds have reasonably good technical properties, including light and weather fastness and resistance to solvents and water. The biological importance of azo complexes is well known due to their use as inflammatory [10], anticancer [11], antibacterial [12], and antifungal [13]. Azo

complexes have received much attention due to their versatile use in many practical applications such as coloring fiber [14].

A qualified plan for this study will be established on the basis of the properties of azo coumarin and its metal complexes which have many different properties. The present work is devoted to the preparation of new complexes of Cu(II), Ni(II) Zn(II) and Mn(II) with 3-Ethoxy-6-(phenyl azo)-7-hydroxy coumarin. Their structures and thermal stability are elucidated by means of partial elemental analysis, spectroscopic (IR, UV-visible and ^{1}H NMR) as well as magnetic measurements. Also, the thermal behavior of the synthesized complexes was investigated using TGA and the corresponding kinetic parameters are evaluated. The calf thymus DNA binding activity of the ligand and its metal complexes were studied by absorption spectra and viscosity measurements. The antitumor activity of the ligand and its metal complexes was tested against human cancer MCF-7 (breast cancer).

2. Materials and methods

2.1. Materials and apparatus

All reagents were purchased from Merck, Aldrich and Fluka and used without any further purification. CT-DNA was purchased from SRL (India). The reagents; RPMI-1640 medium, MTT, DMSO and 5-fluorouracil were purchased from Sigma chemicals (St. Louis, USA). Double distilled water was used to prepare buffer solution. Microanalytical data (C, H and N) were collected on Automatic Analyzer CHNS Vario ELIII, Germany. Spectroscopic data were obtained using the following instruments: FTIR spectra (KBr discs, 4000-400 cm^{-1}) by Jasco FTIR-4100 spectrophotometer; the ^{1}H NMR spectra by Advance DRX 500 Bruker spectrometer (400 MHz) using DMSO-d6 as a solvent containing TMS as the internal standard. UV–Visible spectra by Jenway AA800 spectrophotometer Model AAS. Thermal analysis of the ligand and its complexes were carried out using a Shimadzu thermogravimetric analyzer under a nitrogen atmosphere with heating rate of 10 ^{o}C/min over a temperature range from room temperature up to 1000 ^{o}C. The magnetic moment values were evaluated at room temperature using a Johnson Matthey magnetic susceptibility balance using $Hg[Co(SCN)_4]$ as calibrant. Conductivity measurements of the complexes at 25 ± 1 ^{o}C were determined in DMF (10^{-3} M) using conductivity/TDS meter model Lutron YK-22CT. Conductivity measurements of the complexes at 25 ± 1 ^{o}C were determined in DMF (10^{-3} M) using conductivity/TDS meter model WTW model cond 3110. The molecular structures of the investigated compounds were optimized by HF method with 3-21G basis set. The molecules were built with the Perkin Elmer ChemBio Draw and optimized using Perkin Elmer ChemBio3D software [15].

2.2. Synthesis of 3-Ethoxy-6-(phenyl azo)-7-hydroxy coumarin (HL)

The ligand (**HL**) was prepared in two steps:

Step 1: 3-ethoxy carbonyl-7-hydroxy coumarin (0.01 mol) was prepared via the condensation of 2,4-dihydroxy benzaldehyde with diethyl malonate and ethyl aceto acetate in the presence of the piperidene The medium temperature should be maintained at 5 $^{\circ}C$ by using ice salt bath during addition, and then the reaction mixture was kept at

room temperature overnight, and then poured with vigorous stirring into a mixture crushed ice and water. The solid 3-ethoxy carbonyl-7-hydroxy coumarine was filtered off and washed several times with cold water and recrystallized from ethanol. Elemental analysis: $C_{12}H_9O_5$ (M = 233.21) C 61.87 (calc. 61.80); H 3.99 (3.92); O 34.35 (34.30)% IR (KBr): 3430 υ(OH), 1668 υ(C=O) cm^{-1}. ^1H NMR in DMSO, internal TMS, d (ppm): δ 1.5 (t, 3H, CH_3), 4.25(q, 2H, CH_2), 6.77-7.93 (m, 7H, Ar-H), 8.70 (s, 1H, OH) ppm.

Step 2: A well stirred solution of aniline (0.01 mole) in 10 ml ethanol and 5 ml of 2M HCl was cooled in ice bath and diazotized with aqueous sodium nitrite solution (5 ml, 0.01 mole). The cooled (0-5 ^oC) diazonium solution was added drop wisely to a well stirred solution of (0.01 mole) 3-ethoxy carbonyl-7-hydroxy coumarin in (100 ml) ethanol containing sodium hydroxide (0.01 mole) during 45 minutes. The mixture was stirred for further 30 minutes and then left for 2 hours in refrigerator. The solid product was collected, washed with water, dried and recrystallized with ethanol. Elemental analyses for the prepared coumarin azo dye (Table 1) were done. The structure of the ligand was established by ^1H NMR, mass and IR spectral analysis.

2.3. Synthesis of metal complexes (1-4)

Metal complexes (**1-4)** were synthesized according to the following procedure: methanolic solution of 1 mmol of metal chloride ($CuCl_2.2H_2O$, $NiCl_2.6H_2O$, $ZnCl_2$ and $MnCl_2.4H_2O$) was added dropwise to a hot methanolic solution of 1 mmol of the investigated ligand with stirring. The pH of solution was maintained at a value of 7-8 by addition of dilute ammonia solution and the reaction mixture was refluxed for 3 hrs. The solution was concentrated to half of its original volume by evaporation and allowed to cool at room temperature. During this, a microcrystalline solid (Fig. 1) was filtered off, washed with hot methanol and dried in a vacuum desiccator over anhydrous $CaCl_2$.

2.4. DNA binding experiments

2.4.1. Electronic absorption titrations.

The binding properties of the ligand and its complexes to CT-DNA have been studied using electronic absorption spectroscopy. The stock solution of CT-DNA was

prepared in 5 µM Tris-HCl/50 µM NaCl buffer (pH=7.2), which a ratio of UV absorbances at 260 and 280 nm (A_{260}/A_{280}) of ca. 1.8-1.9, indicating that the DNA was sufficiently free of protein [16], and the concentration was determined by UV absorbance at 260 nm (ε = 6600 $M^{-1}.cm^{-1}$) [17]. Electronic absorption spectra (200-700 nm) were carried out using 1 cm quartz cuvettes at 25 ^{o}C by fixing the concentration of ligand or complex (1.00 x 10^{-4} $mol.L^{-1}$), while gradually increasing the concentration of CT-DNA (0.00 to 1.30 x 10^{-5} $mol.L^{-1}$). An equal amount of CT-DNA was added to both the compound solutions and the references buffer solution to eliminate the absorbance of CT-DNA itself. The intrinsic binding constant K_b of the compound with CT-DNA was determined using the following equation (1) [18]:

$$[DNA] / (\epsilon_a - \epsilon_f) = [DNA] / (\epsilon_b - \epsilon_f) + 1 / K_b(\epsilon_a - \epsilon_f) \quad (1)$$

Where [DNA] is the concentration of CT-DNA in base pairs, ϵ_a is the extinction coefficient observed for the A_{obs}/[compound] at the given DNA concentration, ϵ_f is the extinction coefficient of the free compound in solution and ϵ_b is the extinction coefficient of the compound when fully bond to DNA. In plots of $[DNA]/(\epsilon_a - \epsilon_f)$ *vs.* [DNA], K_b is given by the ratio of the slope to the intercept.

2.4.2. Viscosity measurements.

Viscosity experiments were carried out using an Ubbelodhe viscometer, immersed in a

water bath at 25±0.1 ^{o}C. The viscosity of a 1x10^{-4} M solution of CT-DNA was determined in the presence of the compound, using different [Compound]/[DNA] ratios, in the range of 0.00–1.00 with 0.10 intervals. The flow time for each sample was recorded in triplicate with a digital stopwatch, and an average flow time was calculated [19]. The relative viscosity values (η) were determined (Eq. 2) from the flow time of the DNA-containing solutions (t) corrected by the flow time of the free buffer (t_o):

$$\eta = (t - t_o)/t_o \quad (2)$$

The data are presented as the plot of the relative viscosity, i.e. $(\eta/\eta_o)^{1/3}$ *vs.* [Compound]/[DNA]. η_o and η are the viscosity of the free DNA solution and the DNA–compound solution, respectively.

2.5. Antitumor activity

2.5.1. Cell line

Mammary gland breast cancer (MCF-7) cell line was obtained from ATCC via Holding company for biological products and vaccines (VACSERA), Cairo, Egypt.

2.5.2. MTT assay

The cell line mentioned above was used to determine the inhibitory effects of compounds on cell growth using the MTT assay [20].

$$\%\,\text{The relative cell viability} = \frac{\text{A}\,(570\,\text{nm})\,\text{of treated samples}}{\text{A}\,(570\,\text{nm})\,\text{of untreated sample}} \times 100 \qquad (3)$$

3. Results and discussion

The results of physical properties of the prepared ligand (**HL**) and its metal complexes (**1-4**) along with their elemental analysis are collected in Table 1. The analytical data of metal complexes indicated that the complexes have 1:1 (metal: ligand) stoichiometry. The metal complexes are stable in air and soluble in most common organic solvents. The molar conductance of the synthesized metal complexes was measured in DMF (10^{-3} M) at room temperature. The low conductivity values in the range 5.8-17.6 $\Omega^{-1}cm^{2}mol^{-1}$ may be attributed to the presence of chloride ions in the coordination sphere rather than ionic association to the metal ions during complex formation and also no white precipitate is formed by the addition of $AgNO_3$. This directly supports the fact that all of the investigated complexes are non-ionic or non-electrolytes in nature [21]. The conductivity values for all of the investigated complexes are listed in Table 1.

3.1. IR spectra

The FTIR spectra provide valuable information regarding the nature of the functional group attached to the metal atom. By comparing the IR spectra of the ligand with those of its metal complexes, the following features can be pointed out:

(1) The broad and strong intensity band due to ν(OH) group which appear at 3434 cm^{-1} arises from the strong intra and intermolecular hydrogen bonding of the free ligand [22].

(2) The broad band appeared in the spectra of the complexes in the range 3185-3143 cm^{-1} were attributed to the υ(H_2O) vibration and indicated the involvement of water molecules associated the complex formation (coordination and/or water of hydration).

(3) The medium bands in the region 3090-3040 cm^{-1} are due to Ar-H stretching vibration in the spectra of the ligand and its complexes.

(4) The IR spectrum of the investigated ligand show the -C=C- band at 1600 cm^{-1} , appeared almost at the same position in the spectra of its metal complexes.

(5) The band corresponding to ν(C=O) which appeared in the spectrum of the ligand at 1670 cm^{-1}, appeared almost at the same position in the spectra of its metal complexes [23], which can be taken as evidence that C=O groups are not taking part in the coordination to the metal center.

(6) The band due to ν(N=N) group which appeared in the spectrum of the ligand at 1482 cm^{-1} was shifted to lower wavenumbers by 7-22 cm^{-1} indicating their coordination to the metal center.

(7) The medium band corresponding to phenolic oxygen to ν(C-O) which appeared in the spectrum of the ligand at 1295 cm^{-1}, Upon chelation this band is shifted to lower wavenumber [22], the ligand coordinate through their deprotonated form and formation of metal–oxygen bonds.

(8) In addition, new bands were observed in the regions 514-573 and 437-470 cm^{-1} which were assigned to the formation of M–O and M←N bonds, respectively [24]. This further supports the coordination of the nitrogen atom of the azo group (-N=N-) and oxygen atom of the deprotonated phenolic OH.

3.2 Electronic spectra and magnetic studies

The UV-VIS absorption spectra of **HL** and its metal complexes (**1-4**) within the range of 200-900 nm were scanned and assigned in DMF or Nujol mull (DMF has no

effect on the color). The geometry of the metal complexes has been deduced from electronic spectra and magnetic data of the complexes.

The spectrum of free ligand (**HL**) exhibit two intense bands at 342 and 374 nm due to $\pi \rightarrow \pi^*$ and $n \rightarrow \pi^*$ transitions, respectively [25]. These transitions are shifted to blue or red frequencies due to the coordination of the ligand with metal ions. A change is observed on the spectra of all the complexes due to LMCT from N and O donors.

The electronic absorption spectrum of Cu(II) complex contain an absorption bands at 446 and 336 nm due to the transition ($^2B_{1g} \rightarrow {}^2E_g$) and ($^2B_{1g} \rightarrow {}^2B_{2g}$) in order of decreasing energy, respectively. These indicate a square planar structure around the copper ion [26]. The magnetic moments of Cu(II) complex in any of its geometry lies around 1.85 B.M. which is very close to spin-only value i.e. 1.73 B.M. The values which we found in our case lie at 1.74 B.M. This value is typical for mononuclear copper(II) compound having d^9-electronic configuration (s=½) spin-state. The monomeric nature of the complex is further supported by the microanalytical data.

The magnetic moment of Ni(II) complex is 3.2 B.M. within the high spin octahedral (3.0 – 3.5 B.M.). The high spin data arise from the spin orbit coupling which causes an orbital contribution to the quenched $^3A_{2g}$ ground state of Ni(II) ion in an octahedral structure [27]. Its electronic spectrum shows three bands at 495 (υ_3), 456 (υ_2) and 376 nm (υ_1) which assigned to $^3A_{2g} \rightarrow {}^3T_{1g}$ (P), $^3A_{2g} \rightarrow {}^3T_{1g}$ (F) and $^3A_{2g} \rightarrow {}^3T_{1g}$ (F), respectively, due to octahedral structure [28]. Beside of these three bands, there is a charge transfer band is existed at 734 cm^{-1}.

The electronic absorption spectrum of the diamagnetic Zn(II) complex (d^{10} configuration) show the bands at 438 and 338 nm which are assigned to intra-ligand charge transfer transitions [29].

The magnetic moment of Mn(II) complex was found to be 5.31 B.M., indicating the presence of 5 unpaired electrons in the d-orbital and show a high spin d^5 octahedral geometry for 1:1 complexes. The electronic spectrum of Mn(II) complex shows three bands at 330, 402 and 432 nm due to $^4T_{1g} \rightarrow {}^6A_{1g}$, $^4T_{2g}(G) \rightarrow {}^6A_{1g}$ and $^4T_{1g}(D) \rightarrow {}^6A_{1g}$ transition, respectively [30].

3.3. ^{1}H and ^{13}C-NMR spectra

The investigated ligand (**HL**) and its diamagnetic Zn(II) complex were recorded in DMSO as a solvent. The chemical shift of the investigated ligand (**HL)** as the follow: δ 1.3 (t, 3H, CH_3), 4.21(q, 2H, CH_2), 6.75-7.88 (m, 7H, Ar-H), 8.21(S, 1H, 1H, H_{pyrane} ring), 8.75 (br-S, 1H, OH) ppm. The chemical shift of Zn(II) complex as follows: the disappearance of the signal observed at 8.75 ppm in the free ligand indicates the deprotonation and involvement of the OH group in complexation. Coordinated water molecules were observed in the region 2.85 ppm. All of the other signals observed in the free ligand still present with some up field shift which may be due to complexation.

In the ^{13}C-NMR spectrum of the ligand (**HL**): δ167.00, 165.65 (C=O), 158.39, 151.78, 149.94, 139.21, 137.11, 132.09, 130.126, 129.83, 123.82, 123.23, 118.37, 114.89, 114.43, 110.67, 104.48, (C-aromatic), 61.78 (OCH_2), 14.45 (CH_3) ppm.

3.5. Mass spectral studies

Mass spectral studies of the investigated ligand and its Ni(II) complex permit the elucidation of molecular weight. Mass spectroscopy has proved extremely valuable for the determination of accurate molecular weights, obtaining molecular formulae, ionization potentials and bond strengths.

Mass spectrum of HL

Mass spectrum/z (%): 338(M^+,10.2),311(5.53),310(29.49),293(0.90),267(2.09),266(7.13),238(2.11),234(2.13),233(16.61),212(1.55),210(2.99),206(13.19),205(17.20),190(1.13),189(8.58),188(3.95),187(19.17),178(3.69),177(17.60),163(3.62),162(27.14)161(15.75),160(2.80),159(13.60),152(2.14),150(1.64),149(5.81),135(4.27),134(35.09),133(9.78),132(3.89),128(1.19),127(00.98),121(3.96),120(1.92),119(2.17),118(1.03),117(1.61),107(2.92),106(6.08),105(36.94),104(6.05),103(3.88),94(5.45),93(43.15),92(11.31),91(9.05),89(2.36),87(1.60),81(2.80),79(4.26),78(16.28),77(100),76(10.82),75(7.33),52(5.15),51(29.95),50(8.84),45(3.60),44(27.63),40(56.21).

Mass spectrum of Ni(II) complex:

Mass spectrum/z (%):

503(M^+,5.18),275(1.08),268(2.29),267(11.89),240(3.82),239(8.91),212(1.14),211(1.4),210(5.56),196(1.73),186(12.05),184(2.69),182(1.4),169(2.67),166(1.39),163(7.20),162(66.7),161(2.31),158(3.26),155(2.1),152(1.11),145(1.10),144(5.55),143(4.48),139(1.22),135(10.16),134(100.00),133(5.84),130(1.25)128(3.17),127(2.17),121(1.89)119(2.08),118(2.00),117(2.08),116(4.10),115(4.84),114(3.18),113(1.09),112(1.85),111(1.56),108(6.49),107(4.39),106(14.57),105(37.25),104(3.34),103(3.32),101(2.24),100(1.12),94(3.96),93(36.84),92(10.90),91(7.07),89(6.58),87(4.03),81(5.46),79(14.40),78(67.19),77(58.30),76(11.25),75(8.36),74(11.58),69(22.76),67(12.17),66(23.01),65(22.55),63(40.38),62(25.51),61(12.54),56(3.28),55(11.51),53(16.81),52(22.28),51(49.74),50(29.95),49(4.73),45(8.05),44(73.07),43(15.85),42(13.21),41(16.63),40(4.50).

3.6. Molecular Structure

The molecular structures of the ligand (**HL**) and its metal complexes (**1-4**) were optimized by HF method with 3-21G basis set. The molecules were built with the Perkin Elmer ChemBioDraw and optimized using Perkin Elmer ChemBio3D software. the calculated molecular structures for HL are shown in Fig. 2. The geometrical parameters bond lengths and bond angles of ligand and its metal complexes (**1-4**) are presented in Tables 2-4.

Molecular structure (HOMO & LUMO) for HL is presented in Fig. 3. The HOMO–LUMO energy gap, ΔE, which is an important stability index, is applied to develop theoretical models for explaining the structure and conformation barriers in many molecular systems. The smaller value of ΔE, the more reactivity of the compound [31]. The calculated quantum chemical parameters are given in Table 5. Additional parameters such as separation energies, ΔE, absolute electronegativities, χ, chemical potentials, P_i, absolute hardness, η, absolute softness, σ, global electrophilicity, ω [32], global softness, S, and additional electronic charge, ΔN_{max}, have been calculated according to the following equations (4-11):

$$\Delta E = E_{LUMO} - E_{HOMC} \tag{4}$$

$$\chi = \frac{-(E_{HOMO} + E_{LUMO})}{2} \tag{5}$$

$$\eta = \frac{E_{LUMO} - E_{HOMO}}{2} \quad (6)$$

$$\sigma = 1/\eta \quad (7)$$

$$Pi = -\chi \quad (8)$$

$$S = \frac{1}{2\eta} \quad (9)$$

$$\omega = Pi^2 / 2\eta \quad (10)$$

$$\Delta N_{max} = -Pi/\eta \quad (11)$$

The value of ΔE for the ligand HL was found 1.20, and for Cu(II), Ni(II), Zn(II) and Mn(II) complexes was found 3.50, 0.55, 1.21 and 0.13 eV, respectively. The calculations indicated that the Cu(II) complex is more stable form than the other complexes [33].

3.7. Thermal analyses

The thermal properties of ligand (**HL**) and its metal complexes (**1-4**) were characterized on the basis of thermogravimetric analysis (TGA). The temperature intervals and the percentage of loss of masses of the ligand are listed in Table 6. It is clear that the change of substituent affects the thermal properties of the ligand and its complexes.

The ligand (**HL**) shows four decomposition steps, the first stage occur in the temperature range 45.77 – 381.82 °C is attributed to loss of C_6H_5 (Found 23.39 % and calc. 22.78 %). The second stage in the temperature range 381.82-573.51 °C corresponding to loss of a part of the ligand $C_6H_5ON_2$ (Found 35.92 %, calc. 35.78 %).the third stage occur in the temperature range 573.51 – 783.94 °C corresponding to loss of a part of the ligand $C_5H_4O_2$ (Found 30.43 %, calc. 28.39 %). The fourth stage occur in the temperature range 784.9 – 999.75 °C corresponding to loss of CO (Found 9.68 %, calc. 8.27 %).

Complex (**1**) shows loss of ($C_3H_{11}O_4$), (Found 21.48 %, calc. 22.67 %), occur in the temperature range 45.76 – 254.0 °C, loss of (C_6H_6O), (Found 20.28 %, calc. 19.18 %),

occur in the temperature range 254.71–343.35 °C , loss of ($C_9H_2O_2N_2Cl$+CuO residue) (Found 58.12 %, calc. 58.14 %).

Complex (**2**) shows loss of ($4H_2O$+Cl) , (Found 21.11 %, calc. 21.34 %), occur in the temperature range 45.87 – 267.17 °C, loss of ($C_{18}H_{10}O_5N_2$), (Found 62.54 %, calc. 66.39 %), occur in the temperature range 267.55 – 431.07 °C NiO residue, (Found 12.59 %, calc. 14.83 %), occur in the temperature range 432.08–999.84 °C.

Complex (**3**) shows loss of ($C_3H_9O_3Cl$), (Found 29.49 %, calc. 27.20 %), occur in the temperature range 47.84 – 369.99 °C, loss of ($C_{12}H_6ON_2$), (Found 39.41 %, calc. 41.0 %), occur in the temperature range 370.34 – 451.78 °C. Loss of $C_3H_2O_2$+ZnO residue, (Found 30.90 %, calc. 32.0 %), occur in the temperature range 452.15 – 623.0 °C .

Complex (**4**) shows loss of ($2H_2O$+C_2H_5), (Found 12.32 %, calc. 13.01 %), occur in the temperature range 45.81–220.42 °C. Loss of ($C_9H_4O_3N_2Cl$), (Found 44.34 %, calc. 44.72 %), occur in the temperature range 221.15 – 410.38 °C. Loss of $C_7H_3O_4$ + MnO residue, (Found 43.28 %, calc. 44.41 %), occur in the temperature range 410.60 – 999.17 °C.

3.8. Calculation of activation thermodynamic parameters

The thermodynamic activation parameters of decomposition processes of the ligand (HL) and its metal complexes namely activation energy (E_a), enthalpy (ΔH^*), entropy (ΔS^*), and Gibbs free energy change of the decomposition (ΔG^*) are evaluated graphically by employing the Coast-Redfern [34] and Horowitz-Metzger [35] methods.

Coast-Redfern equation

The Coast-Redfern equation, which is a typical integral method, can represent as:

$$\int_0^a \frac{dx}{(1-\alpha)^n} = \frac{A}{\varphi}\int_{T_1}^{T_2} \exp\left(-\frac{E_a}{RT}\right)dt \qquad (12)$$

For convenience of integration, the lower limit T_1 usually taken as zero. This equation on integration gives:

$$\ln\left[-\frac{\ln(1-\alpha)}{T^2}\right]=-\frac{E_a}{RT}+\ln\left[\frac{AR}{\varphi\ E_a}\right] \tag{13}$$

A plot of left-hand side (LHS) against 1/T was drawn Fig. 4. E_a is the energy of activation in $J.mol^{-1}$ and calculated from the slope and A in (s^{-1}) from the intercept value. The entropy of activation (ΔS^*) in ($J.mol^{-1}.K^{-1}$) calculated by using the equation:

$$\Delta S^* = 2.303\left[\log\left(\frac{Ah}{k_B T_s}\right)\right]\mathrm{R} \tag{14}$$

Where k_B is the Boltzmann constant, h is the Plank's constant and T_s is the TG peak temperature.

Horowitz-Metzger equation

The Horowitz-Metzger equation is an illustrative of the approximation methods. These authors derived the relation:

$$\log\left[\frac{1-(1-\alpha)^{1-n}}{1-n}\right]=\frac{E_a\theta}{2.303RT_s^2}, \text{ for } n\neq 1 \tag{15}$$

when n = 1, Eq. (15) would be log[-log(1-α)] (Fig. 5). For a first order kinetic process, the Horowitz-Metzger equation may write in the form:

$$\log\left[\log\left(\frac{W\alpha}{W\gamma}\right)\right]=\frac{E_a\theta}{2.303RT_s^2}-\log 2.303 \tag{16}$$

where θ = T-Ts, w_γ = wα- w, wα = mass loss at the completion reaction; w = mass loss up to time t. The plot of log [log ($w\alpha/w_\gamma$)] *vs.* θ was drawn and found to be linear from the slope of which E_a was calculated. The pre-exponential factor, A, calculated from equation:

$$\frac{E_a}{RT_s^2} = \frac{A}{\left[\varphi \ \exp\left(-\frac{E_a}{RT_s}\right)\right]} \tag{17}$$

The entropy of activation, ΔS^*, is calculated from Eq. (14). The enthalpy activation, ΔH^*, and Gibbs free energy, ΔG^*, calculated from:

$$\Delta H^* = E_a - RT \tag{18}$$

$$\Delta G^* = \Delta H^* - T\,\Delta S^* \tag{19}$$

The calculated values of E_a, A, ΔS^*, ΔH^* and ΔG^* for the decomposition steps for ligand (**HL**) and its metal complexes (**1-4**) are summarized in Table 7.

3.9. DNA binding studies

3.9.1. Electronic absorption studies of DNA binding

Absorption titration is one of the most universally employed methods to study the binding modes and binding extent of compounds to DNA. Absorption titration experiments were performed with fixed concentrations of the ligand (**HL**) and its metal complexes (**1-4**) (40 μM) while gradually increasing the concentration of DNA (10 μM) at 25 °C. While measuring the absorption spectra, an equal amount of DNA was added to both the compound solution and the reference solution to eliminate the absorbance of DNA itself. We have determine the intrinsic binding constant to CT-DNA by monitoring the absorption intensity of the charge transfer spectral band at 330 nm for the ligand (**HL**) and 325, 420, 450, 325 nm for (**1**), (**2**), (**3**) and (**4**) complexes, respectively.

The absorption spectra of **HL** and its metal complexes (**1-4**) with increasing concentration of CT-DNA in the range 280-600 nm are shown in Figs. 6 and 7. Upon the addition of increasing amount of CT-DNA, a significant “hyperchromic” effect was observed accompanied by a moderate red shift of 2–3 nm, indicative of stabilization of the DNA helix. These spectral characteristic suggest that the ligands and complexes bind either to the external contact (electrostatic binding) or to the major and minor grooves of

DNA. Moreover, this "hyperchromic effect" can be explained on the basis of two phenomena. Firstly, the large surface area of the ligand as well as presence of planar aromatic chromophore facilitates a strong binding interaction of the ligands with CT-DNA there by, providing ample opportunity for the complex to bind with the CT-DNA via, partial insertion of the aromatic moiety in between the stacking base pair [36].

The intrinsic binding constants (K_b) of the ligand (**HL**) and its metal complexes (**1-4**) with CT-DNA were determined (Eq. 1) [37].

The K_b values obtained from the absorption spectral technique for ligand (**HL**) was calculated as 1.24×10^5 M^{-1}. The K_b values obtained from the absorption spectral technique for metal complexes were calculated as 2.25×10^5, 3.18×10^5, 5.12×10^5 and 5.82×10^5 M^{-1} for (**1**), (**2**), (**3**) and (**4**) complexes, respectively. The binding constant of the complexes are comparatively higher than that of the ligand, may be due to the ligand considering that the phenolic -OH group may enhance their affinity towards DNA binding through formation of hydrogen bonding.

3.9.2. Viscosity measurements

Due to its sensitivity to the change of length of DNA, viscosity measurement may be the most effective means to study the binding mode of a complex to DNA. A significant increase in the viscosity of DNA on the addition of a complex indicates the classical intercalative mode of binding to DNA. In contrast, a complex that binds in the DNA grooves by partial and/or non-classical intercalation causes less pronounced (positive or negative) or no change in DNA solution viscosity [38].

The relative specific viscosity of DNA was determined at 25 ^oC by increasing the concentration of the metal complexes (**1-4**) from 0-200 µM, while the CT-DNA concentration (200 µM) was kept constant. Viscosity experimental results clearly showed that the relative viscosity of CT-DNA increases steadily on addition of increasing concentration of the complexes (**1-4**). The increased degree of viscosity, which may depend on its affinity to DNA follows the order of **1** > **2** > **4** > **3**. This observation can be explained on the fact that, classical intercalation model demands that the DNA helix must lengthen as base pairs are separated to accommodate the binding complexes, leading to the increase of DNA viscosity, as for the behaviors of the known DNA intercalators [39].

3.10. Molecular docking

Cancer can be described as the uncontrolled growth of abnormal cells. Prostate cancer is the most common non-skin malignancy in men. Except for lung cancer, it is responsible for more deaths than any other cancer. The American Cancer Society (ACS) estimated 1 man in 6 will be diagnosed with prostate cancer during his lifetime. A little over 1.8 million men in the United States are survivors of prostate cancer [40].

Breast cancer is one of the most recurring worldwide diagnosed and deadliest cancers next to lung cancer with a high number of mortality rates among females [41]. At global level, it accounted for more than 1.6 million new cases in 2010. The incidence or prevalence rate of the breast cancer in India is expected to be more than 90,000 in the coming years and over 50,000 women die each year.

Docking study showed the binding affinity, number of hydrogen bonds. It is interesting to note that the binding affinities have negative values. This reveals the high feasibility of this reaction. Molecular docking is a key tool in computer drug design [42]. The focus of molecular docking is to simulate the molecular recognition process. Molecular docking aims to achieve an optimized conformation for both the protein and drug with relative orientation between them such that the free energy of the overall system is minimized.

The study simulates the actual docking process in which the ligand–protein pair-wise interaction energies are calculated using Docking Server [43]. The MMFF94 Force field was used for energy minimization of ligand molecules using Docking Server. Gasteiger partial charges were added to the ligand atoms. Non-polar hydrogen atoms were merged, and rotatable bonds were defined. Docking calculations were carried out on 3hb5 and 2q7k –oxidreductase–Hormone protein model. Essential hydrogen atoms, Kollman united atom type charges, and solvation parameters were added with the aid of AutoDock tools [44]. Affinity (grid) maps of 20X20X20 Å grid points and. 375 Å spacing was generated using the Autogrid program [45]. Auto Dock parameter set- and distance-dependent dielectric functions were used in the calculation of the van der Waals and the electrostatic terms, respectively.

Docking simulations were performed using the Lamarckian genetic algorithm (LGA) and the Solis & Wets local search method [46]. Initial position, orientation, and torsions of the ligand molecules were set randomly. All rotatable torsions were released during docking. Each docking experiment was derived from 10 different runs that were set to terminate after a maximum of 250000 energy evaluations. The population size was set to 150. During the search, a translational step of 0.2 Å, and quaternion and torsion steps of 5 were applied.

In this context, the docked ligand was analyzed with the breast Censer mutant 3hb5 and prostate cancer 2q7k–Hormone as shown in Figs. 8(A), (B) and 9(C), (D). The study simulates the actual docking process in which the ligand – protein pair-wise interaction energies are calculated in Tables 8 and 9. According to our results, , HB plot curve indicates that, azo compound binds to the two proteins with hydrogen bond interactions of ligand (**HL**) with 3hb5 and 2q7k as shown in Figs. 10 and 11. The calculated efficiency is favorable, K_i values estimated by AutoDock were compared with experimental K_i values, when available, and the Gibbs free energy is negative. Also, based on this data, we can propose that interaction between the 3hb5 and 2q7k receptors and the ligand (**HL**) is possible. 2D plot curve of docking with ligand (**HL**) is shown in Figs. 12 and 13. This interaction could activate apoptosis in cancer cell energy of interactions with ligand (**HL**). From the analysis of the values, it is evident that the binding energy of (**HL**) decreases. So that is increase in binding energy of (**HL**) on transpiration of mutation for for breast cancer whereas decrease with prostate cancer 2q7k. Binding energies are most widely used mode of measuring binding affinity of a ligand. Thus, the decrease in binding energy due to mutation will increase the binding affinity of the azo coumarin ligand towards the receptor. The characteristic feature of azo coumarin represents the presence of several active sites available for hydrogen bonding. This feature gives them the ability to be good binding inhibitors to the protein and will help to produce augmented inhibitory compounds. The results confirm that, the azo dye ligand is an efficient inhibitor of 3hb5–oxidoreductase breast cancer and prostate cancer mutant 2q7k–Hormone.

3.11. Antitumor activity

In vitro antitumor activity of the tested ligand (**HL**) and its metal complexes (**1-4**) was assayed for their cytotoxicity against human breast cancer (MCF-7) by MTT assay [20]. The inhibitory activity against breast cancer cells (MCF-7) was detected by using different concentrations of the tested samples (0.00, 0.10, 1.0, 10.00, 100.00 and 1000.00 µg/ml) and cell viability (%) was determined at 540 nm using a microplate reader. The IC_{50} of tested compounds was calculated from Table 10.

The antitumor results of the ligand (**HL**) and its metal complexes are listed in Table 11. As shown in Table 11 the complexes (**1**), (**3**) and (**4**) displayed good activity on MCF-7 cells comparing with the ligand (**HL**) (IC_{50} = 30.00 µg/ml). In the case of MCF-7 cells of complex (**2**) showed cytotoxicity activity.

4. Conclusion

The structures of Cu(II), Ni(II), Zn(II) and Mn(II) complexes (**1-4**) of the ligand (HL) were confirmed by elemental analyses, IR, ^{1}H NMR, molar conductance and thermal analysis data. IR spectra of the complexes (**1-4**) concluded that **HL** binds to the metals as a monobasic bidentate ligand by coordinating via the nitrogen atom of the azo group (-N=N-) and oxygen atom of the deprotonated phenolic OH group. The optimized bond lengths, bond angles and calculated the quantum chemical parameters for the ligand (**HL**) and its complexes were investigated. The thermogravimetric analysis of the compounds shows that the values of activation energies of decomposition (E_a) is 49.2 kJ mol^{-1} for the ligand and the values of E_a are found to be 77.0 , 22.1, 23.20 and 66.40 kJ.mol^{-1} for the complexes of Cu(II), Ni(II), Zn(II) and Mn(II), respectively. The calf thymus DNA binding activity of the ligand (**HL**) and its metal complexes (**1-4**) was studied by absorption spectra and viscosity measurements. The ligand (**HL**) considering that the phenolic -OH group may enhance their affinity towards DNA binding through formation of hydrogen bonding. Molecular docking and binding energy calculations of **HL** with the receptor of breast cancer 3hb5–oxidoreductase and prostate cancer mutant 2q7k–Hormone was studied indicated that the presence of the azo coumarin is an efficient inhibitor of breast cancer 3hb5–oxidoreductase and prostate cancer mutant 2q7k–Hormone. The ligand (**HL**) and its metal complexes displayed good activity on MCF-7 cells.

References

[1] L. Pari, N. Rajarajeswari, J. Chem.-Biolog. Interaction 181(3) (2009) 292–296.

[2] L. Raev, E. Voinov, I. Ivanov, D. Popov, J. Pharm. 45 (1990) 696–702.

[3] A.M. El-Agrody, M.S Abd El-Latif, A.H. El-Hady, N.A. Fakery, A.H. Bedair, J. Molecules 6 (2001) 519–527.

[4] T. Patonay, G.Y. Litkei, R. Bognar, J. Erdei, C. Misztic, J. Pharm. 39(2) (1984) 86-91.

[5] A.F. El-Farargy, Egypt. J. Pharm. Sci. 32 (1991) 625–632.

[6] A.A.E. Giota, K.C. Fylaktakidou, D.L.H. Litina, K. ELitinas, D.N. Nicolaides, J. Heterocyc. Chem. 38(3) (2001) 717–722.

[7] R. O'kennedy, R.D. Thornes, "Coumarins – Biology, Applications and Mode of Action", John Wiley & Sons Ltd., Chichester; Eds, p. 315 (1997).

[8] P.M. Bedi, V. Kumar, M.P. Mahajan, J. Bio. Org. Medic. Chem. Let. 14 (2004) 5211–5213.

[9] J.O. Otutu, J. Chem. Soc. Nig. 33 (2008) 205–212.

[10] D.A. Kennedy, N. Vembu, F.R. Fronczek, M. Devocelle, J. Org. Chem. 76(23) (2011) 9641–9647.

[11] T.A. Farghaly, Z.A. Abdallah, J. Arkivoc 17 (2008) 295–305.

[12] H.N. Chopde, S.J. Meshram, R. Pagadala, A.J. Mungole, J. Int. Chem. Tech. Res. 2(3) (2010) 1823–1830.

[13] J. Sahoo, S. Kumar, P.S. Kumar, J. Taibah Univ. Sci. 9 (2015) 187–195.

[14] B.R. Pandya, Y.K. Agrawal, J. Dyes Pigm. 52 (2002) 161–168.

[15] N.A. El-Ghamaz, M.A. Diab, A.A. El-Bindary, A.Z. El-Sonbati, H.A. Seyam, J. Mater. Sci. Semicond. Proc. 27 (2014) 521–531.

[16] M.J. Waring, J. Mol. Biol. 13 (1965) 269-282.

[17] M.F. Reichmann, C.A. Rice, C.A. Thomos, P. Doty, J. Am. Chem. Soc. 76 (1954) 3047–3053.

[18] A. Wolfe, G.H. Shimer, T. Meehan, J. Biochem. 26 (1987) 6392–6396.

[19] G. Cohen, H. Eisenberg, Biopolym. 8 (1969) 45–55.

[20] T. Mosmann, J. Immunol. Methods 65 (1983) 55–63.

[21] M. Eriksson, M. Leijon, C. Hiort, B. Norden, A. Gradsland, J. Biochem. 33 (1994) 5031–5040.

[22] S. Daravath, M.P. Kumar, A. Rambabu, N. Vamsikrishna, N. Ganji, Shivaraj, J. Mol. Struct. 1144 (2017) 147–158.

[23] A.Z. El-Sonbati, M.A Diab, A.A. El-Bindary , A.F.Shoair , M.A. Hussein , R.A. El-Boz, J. Mol. Struct. 1141 (2017) 186–-203.

[24] K. Nakamato, "Infrared and raman spectra of inorganic and coordination compounds", Wiley-Interscience, New York, 1971.

[25] E. Pahontu, F. Julea, Y. Chumakov, P. Petrenco, T. Rosu, A. Gulea, J. Organomet. Chem. 836–837 (2017) 44–55.

[26] A.B.P. Lever, "Inorganic Electronic Spectroscopy", Elsevier, New York, 1968.

[27] C. Justin Dhanaraj, J. Johnson, Mater. Sci. Eng. C 78 (2017) 1006–1015.

[28] R.A. Lal, S. Choudhury, A. Ahmed, M. Chakaraborty, R. Borthakur, A. Kumar, J. Coord. Chem. 62 (2009) 3864–3874.

[29] E.L. Araújoa, H.F.G.Barbosaa,E.R.Dockalb, É.T.G.Cavalheiroa, J. Biol. Macr. 95 (2017) 168–176.

[30] K.S. Patel, J.C. Patel, H.R., V.K. Patel, K.D. Patel, O. J. Metal 2 (2012) 49–59.

[31] S. Layek, B. Agrahari, A. Tarafdar, C. Kumari, Anuradha, R. Ganguly, D.D. Pathak, J. Mol. Struct. 1141 (2017) 428–435.

[32] M.A. Diab, A.A. El-Bindary, A.Z. El-Sonbati, O.L. Salem, J. Mol. Struct. 1007 (2012) 11–19.

[33] M. Jafari, M. Salehi, M. Kubicki, A. Arab, A. Khaleghian, Inorg. Chim. Acta 462 (2017) 329–335.

[34] A.W. Coats, J.P. Redfern, J. Nature 20 (1964) 68–79.

[35] H.W. Horowitz, G. Metzger, J. Anal. Chem. 35 (1963) 1464–1468.

[36] M. Mohanraj, G. Ayyannan, G. Raja, C. Jayabalakrishnan, Appl. Organomet. Chem. 31(4) (2017) e3582.

[37] L.H. Abdel-Rahman, A.M. Abu-Dief, N.M. Ismail, M. Ismael, J. Inorg. Nano-Metal Chem. 47 (2017) 467–480.

[38] M.P. Kesavan, G.G. Vinoth Kumar, J. Dhaveethu Raja, J. Photochem. Photobiol. B: Biology 167 (2017) 20–28.

[39] L.H. Abdel-Rahman, A.M. Abu-Dief, H. Moustafa, S.K. Hamdan, Appl. Organomet. Chem. 31 (2017) e 3555.

[40] American Cancer Society, Cancer Facts & Figures, American Cancer Society, Atlanta, 2014.

[41] J.R. Benson, I. Jatoi, J. Future Oncol. 8 (2012) 697–702.

[42] N.M. Hosny, M.A. Hussien , F.M. Radwan, N. Nawar, Spectrochim. Acta A 132 (2014) 121–129.

[43] Y. K. Abdel-Monem, S.A. Abou El-Enein, M.M. El-Sheikh-Amer, J. Mol. Struct. 1127 (2017) 386-396.

[44] T.A. Halgren, J. Comput. Chem. 17 (1998) 490–519.

[45] G.M. Morris, D.S. Goodsell, J. Comput. Chem. 19 (1998) 1639–1662.

[46] F.J. Solis, R.J.B. Wets, J. Mathemat. Operat. Res. 6 (1981) 19–30.

Table 1. Physical properties and elemental analysis data of the ligand (**HL**) and its metal complexes (**1-4**).

	Mol. formula	Molecular Weight	Color	M.P (°C)	Yield %	Cald.(Found)%			Mol.Cond. $\mu^{-1}cm^2mol^{-1}$	$\mu_{eff.}$ B.M.
						C	H	N		
HL	$C_{18}H_{14}N_2O_5$	338.52	Red	146	78	63.91(63.88)	5.07(4.90)	8.28(8.32)	-	-
1	$[CuLCl(OH_2)]2H_2O$	490.55	Redish brown	>300	81	44.10(43.92)	3.91(3.70)	5.71(5.83)	12.4	1.85
2	$[NiLCl(OH_2)_3]\ H_2O$	503.71	Redish brown	>300	79	42.95(42.65)	4.21(4.10)	5.56(5.64)	8.6	3.2
3	$[ZnLCl(OH_2)]\ H_2O$	474.39	Redish brown	>300	82	45.61(45.32)	3.62(3.47)	5.906.30)	5.8	diam.
4	$[MnLCl(OH_2)_3]\ H_2O$	499.97	Brown	>300	88	43.27(43.10)	4.24(3.97)	5.60(5.51)	17.60	5.31

Table 2. Bond length of the ligand (**HL**).

Atoms (**HL**)	Length (Å)	Atoms (**HL**)	Length (Å)	Atoms (**HL**)	Length (Å)
C(25)-H(39)	1.115	C(9)-C(14)	1.349	H(36)-C(24)-H(35)	107.789
C(25)-H(38)	1.115	C(9)-C(10)	1.352	H(36)-C(24)-C(25)	111.111
C(24)-H(37)	1.114	N(8)-C(9)	1.270	H(35)-C(24)-C(25)	110.975
C(24)-H(36)	1.114	N(7)-N(8)	1.249	C(25)-O(23)-C(20)	119.733
C(24)-H(35)	1.114	C(6)-H(30)	1.103	O(23)-C(20)-O(22)	117.194
C(24)-C(25)	1.526	C(5)-N(7)	1.267	O(23)-C(20)-C(18)	119.952
O(23)-C(25)	1.403	C(5)-C(6)	1.348	O(22)-C(20)-C(18)	122.854
C(20)-O(23)	1.378	C(4)-H(29)	1.105	H(34)-C(19)-C(18)	120.224
C(20)-O(22)	1.216	C(4)-C(5)	1.348	H(34)-C(19)-C(13)	115.977
C(19)-H(34)	1.103	C(3)-H(28)	1.103	C(18)-C(19)-C(13)	123.799
C(18)-C(20)	1.377	C(3)-C(4)	1.342	C(20)-C(18)-C(19)	117.630
C(19)-C(18)	1.350	C(2)-H(27)	1.103	C(20)-C(18)-C(17)	126.010
C(17)-O(21)	1.218	C(2)-C(3)	1.341	C(19)-C(18)-C(17)	116.359
C(18)-C(17)	1.373	C(1)-H(26)	1.103	O(21)-C(17)-C(18)	123.213
C(17)-O(16)	1.374	C(1)-C(6)	1.343	O(21)-C(17)-O(16)	114.834
O(15)-H(33)	0.966	C(1)-C(2)	1.341	C(18)-C(17)-O(16)	121.953
C(14)-H(32)	1.106	H(39)-C(25) H(38)	110.150	C(17)-O(16)-C(12)	117.555
C(13)-C(19)	1.344	H(39)-C(25)-C(24)	109.585	H(33)-O(15)-C(10)	113.413
C(14)-C(13)	1.345	H(39)-C(25)-O(23)	109.454	H(32)-C(14)-C(13)	118.333
O(16)-C(12)	1.361	H(38)-C(25)-C(24)	109.620	H(32)-C(14)-C(9)	118.816
C(13)-C(12)	1.340	H(38)-C(25)-O(23)	109.439	C(13)-C(14)-C(9)	122.852
C(11)-H(31)	1.104	C(24)-C(25)-O(23)	108.568	C(19)-C(13)-C(14)	122.267
C(12)-C(11)	1.343	H(37)-C(24)-H(36)	107.909	C(19)-C(13)-C(12)	118.302
C(10)-O(15)	1.364	H(37)-C(24)-H(35)	107.791	C(14)-C(13)-C(12)	119.431
C(11)-C(10)	1.345	H(37)-C(24)-C(25)	111.113	O(16)-C(12)-C(13)	122.031

Table 3. Bond angle for the ligand (**HL**).

Atoms(**HL**)	angle(º)	Atoms(**HL**)	angle(º)
H(35)-C(24)-C(25)-O(23)	-179.982	C(19)-C(13)-C(12)-C(11)	-179.983
H(35)-C(24)-C(25)-H(38)	60.516	C(19)-C(13)-C(12)-O(16)	0.011
H(35)-C(24)-C(25)-H(39)	-60.481	C(13)-C(12)-C(11)-C(10)	-0.010
H(36)-C(24)-C(25)-O(23)	-60.064	C(13)-C(12)-C(11)-H(31)	179.998
H(36)-C(24)-C(25)-H(38)	-179.567	O(16)-C(12)-C(11)-C(10)	179.996
H(36)-C(24)-C(25)-H(39)	59.436	O(16)-C(12)-C(11)-H(31)	0.004
H(37)-C(24)-C(25)-O(23)	60.097	C(9)-C(10)-O(15)-H(33)	-0.239
H(37)-C(24)-C(25)-H(38)	-59.405	C(11)-C(10)-O(15)-H(33)	179.727
H(37)-C(24)-C(25)-H(39)	179.597	C(12)-C(11)-C(10)-C(9)	-0.017
C(20)-O(23)-C(25)-C(24)	179.663	C(12)-C(11)-C(10)-O(15)	-179.985
C(20)-O(23)-C(25)-H(38)	-60.722	H(31)-C(11)-C(10)-C(9)	179.976
C(20)-O(23)-C(25)-H(39)	60.080	H(31)-C(11)-C(10)-O(15)	0.007
C(18)-C(20)-O(23)-C(25)	-179.649	N(8)-C(9)-C(14)-C(13)	179.981
O(22)-C(20)-O(23)-C(25)	0.293	N(8)-C(9)-C(14)-H(32)	-0.011
C(17)-C(18)-C(20)-O(22)	0.019	C(10)-C(9)-C(14)-C(13)	-0.023
C(17)-C(18)-C(20)-O(23)	179.957	C(10)-C(9)-C(14)-H(32)	179.985
C(19)-C(18)-C(20)-O(22)	-179.975	N(8)-C(9)-C(10)-C(11)	-179.973
C(19)-C(18)-C(20)-O(23)	-0.036	N(8)-C(9)-C(10)-O(15)	-0.007
C(13)-C(19)-C(18)-C(17)	-0.003	C(14)-C(9)-C(10)-C(11)	0.032
C(13)-C(19)-C(18)-C(20)	179.991	C(14)-C(9)-C(10)-O(15)	179.998
H(34)-C(19)-C(18)-C(17)	179.998	N(7)-N(8)-C(9)-C(10)	0.039
H(34)-C(19)-C(18)-C(20)	-0.008	N(7)-N(8)-C(9)-C(14)	-179.966
C(19)-C(18)-C(17)-O(16)	0.007	C(5)-N(7)-N(8)-C(9)	179.985
C(19)-C(18)-C(17)-O(21)	-179.997	C(4)-C(5)-N(7)-N(8)	-179.986
C(20)-C(18)-C(17)-O(16)	-179.986	C(6)-C(5)-N(7)-N(8)	0.018
C(20)-C(18)-C(17)-O(21)	0.009	C(4)-C(5)-C(6)-C(1)	-0.010
C(18)-C(17)-O(16)-C(12)	-0.003	C(4)-C(5)-C(6)-H(30)	-179.999
O(21)-C(17)-O(16)-C(12)	-179.999	N(7)-C(5)-C(6)-C(1)	179.986
C(12)-C(13)-C(19)-C(18)	-0.006	N(7)-C(5)-C(6)-H(30)	-0.003
C(12)-C(13)-C(19)-H(34)	179.993	C(3)-C(4)-C(5)-C(6)	0.005
C(14)-C(13)-C(19)-C(18)	179.991	C(3)-C(4)-C(5)-N(7)	-179.991
C(14)-C(13)-C(19)-H(34)	-0.010	H(29)-C(4)-C(5)-C(6)	179.999
C(9)-C(14)-C(13)-C(12)	-0.004	H(29)-C(4)-C(5)-N(7)	0.003
C(9)-C(14)-C(13)-C(19)	180.000	C(2)-C(3)-C(4)-C(5)	0.007
H(32)-C(14)-C(13)-C(12)	179.988	C(2)-C(3)-C(4)-H(29)	-179.987
H(32)-C(14)-C(13)-C(19)	-0.009	H(28)-C(3)-C(4)-C(5)	179.994
C(17)-O(16)-C(12)-C(11)	179.987	H(28)-C(3)-C(4)-H(29)	-0.000
C(17)-O(16)-C(12)-C(13)	-0.006	C(1)-C(2)-C(3)-C(4)	-0.014
C(14)-C(13)-C(12)-C(11)	0.020	C(1)-C(2)-C(3)-H(28)	179.999
C(14)-C(13)-C(12)-O(16)	-179.986	H(27)-C(2)-C(3)-C(4)	179.979

Table 4. Bond length of the complexes **(1-4).**

1	Length (Å)	**2**	Length (Å)	**3**	Length (Å)	**4**	Length (Å)
O(29)-H(48)	0.944	O(32)-H(57)	0.941	O(29)-H(46)	0.944	O(31)-H(52)	0.941
O(29)-H(47)	0.942	O(32)-H(56)	0.941	O(29)-H(45)	0.944	O(31)-H(51)	0.941
N(14)-H(34)	1.050	O(31)-H(55)	0.940	O(28)-H(44)	0.940	O(30)-H(50)	0.940
N(14)-H(33)	1.049	O(31)-H(54)	0.940	O(28)-H(43)	0.945	O(30)-H(49)	0.940
O(7)-C(4)	1.362	O(30)-H(53)	0.940	O(7)-C(4)	1.362	O(29)-H(48)	0.940
C(8)-O(7)	1.371	O(30)-H(52)	0.940	C(8)-O(7)	1.371	O(29)-H(47)	0.940
N(22)-C(23)	1.270	O(29)-H(51)	0.943	C(12)-O(24)	1.218	O(28)-H(46)	0.941
C(21)-N(22)	1.264	O(29)-H(50)	0.941	Zn(22)-Cl(23)	2.240	O(28)-H(45)	0.941
C(12)-O(17)	1.218	N(14)-H(37)	1.049	O(13)-Zn(22)	1.892	O(7)-C(4)	1.362
Cu(15)-Cl(16)	2.160	N(14)-H(36)	1.049	N(15)-C(16)	1.267	C(8)-O(7)	1.371
O(13)-Cu(15)	1.811	O(7)-C(4)	1.362	N(14)-N(15)	1.249	C(12)-O(24)	1.218
C(1)-N(14)	1.268	C(8)-O(7)	1.371	C(1)-N(14)	1.270	Mn(22)-Cl(23)	2.160
C(2)-O(13)	1.371	N(22)-C(23)	1.270	C(2)-O(13)	1.373	O(13)-Mn(22)	1.814
C(9)-C(12)	1.377	C(21)-N(22)	1.264	C(9)-C(12)	1.377	N(15)-C(16)	1.269
C(8)-O(11)	1.217	C(12)-O(17)	1.218	C(8)-O(11)	1.217	N(14)-N(15)	1.250
C(12)-O(18)	1.373	Ni(15)-Cl(16)	2.140	C(12)-O(25)	1.373	C(1)-N(14)	1.271
O(18)-C(20)	1.403	O(13)-Ni(15)	1.792	O(25)-C(27)	1.403	C(2)-O(13)	1.377
C(19)-C(20)	1.526	C(1)-N(14)	1.268	C(26)-C(27)	1.526	C(9)-C(12)	1.377
		C(2)-O(13)	1.371			C(8)-O(11)	1.217
		C(9)-C(12)	1.377			C(12)-O(25)	1.373
		C(8)-O(11)	1.217			O(25)-C(27)	1.403
		C(12)-O(18)	1.373			C(26)-C(27)	1.526
		O(18)-C(20)	1.403				
		C(19)-C(20)	1.526				

Table 5. The calculated quantum chemical parameters for the investigated ligand (**HL**) and its metal complexes **(1-4).**

	E_{HUMO} eV	E_{LUMO} eV	ΔE eV	X eV	η eV	δ eV	Pi eV	σ eV^{-1}	S eV^{-1}	Ω eV	ΔN max
HL	-5.27	-4.06	1.20	4.66	0.60	1.66	-4.66	0.30	0.30	2.33	7.76
1	-8.50	-4.99	3.50	6.74	1.75	0.57	-6.74	0.87	0.87	3.37	3.85
2	-9.09	-8.53	0.55	8.81	0.27	3.60	-8.81	0.13	0.13	4.40	31.77
3	-5.34	-4.12	1.21	4.73	0.60	1.65	-4.73	0.30	0.30	2.36	7.82
4	-11.67	-11.53	0.13	11.60	0.06	14.59	-11.60	0.03	0.034	5.80	169.41

Table 6. The thermal analyses data for ligand (**HL**) and its metal complexes **(1-4).**

Compounds	Temp. range °C	Mass loss % Found	Mass loss % Calc.	Assignment
HL	45.77 – 381.82	23.39	22.78	Loss of C_6H_5
	381.82 – 573.51	35.92	35.78	Loss of $C_6H_5ON_2$
	573.51 – 783.94	30.43	28.39	Loss of $C_5H_4O_2$
	784.9 – 999.75	9.68	8.27	Loss of CO
1	45.76- 254.0	21.48	22.67	Loss of $C_3H_{11}O_4$
	254.71 – 343.35	20.28	19.18	Loss of C_6H_6O
	344.17 – 750.0	58.12	58.14	Loss of $C_9H_2O_2N_2Cl$+CuO residue
2	45.87 - 267.17	21.11	21.34	Loss of $4H_2O$+Cl
	267.55 – 431.07	62.54	66.39	Loss of $C_{18}H_{10}O_5N_2$
	432.03 – 999.84	12.59	14.83	NiO residue
3	47.81 – 369.99	29.49	27.20	Loss of $C_3H_9O_3Cl$
	370.34 – 451.78	39.41	41.0	Loss of $C_{12}H_6ON_2$
	452.15 – 623.0	30.90	32.0	Loss of $C_3H_2O_2$+ZnO residue
4	45.81 – 220.42	12.32	13.01	Loss of $2H_2O+C_2H_5$
	221.15 – 410.38	44.34	44.72	Loss of $C_9H_4O_3N_2Cl$
	410.60 – 999.17	43.28	44.41	Loss of $C_7H_3O_4$ + MnO residue

Table 7. Kinetic parameters of the ligand (**HL**) and its metal complexes (**1-4**).

Comp.	Temp. (°C)	Method	Parameters					**R**
			E_a (kJ mol^{-1})	A (s^{-1})	$-\Delta S^*$ ($J.mol^{-1}.K^{-1}$)	ΔH^* (kJ mol^{-1})	ΔG^* (kJ mol^{-1})	
HL	45-187	CR	49.2	2.53 x10	$2.40X10^2$	$4.59X10^4$	$1.42X10^5$	0.95
		HM	44.5	$6.80\ x10^3$	$1.74X10^2$	$4.12X10^4$	$1.11X10^5$	0.99
1	45-118	CR	77.0	$1.38\ x10^8$	$9.11X10^1$	$7.39X10^4$	$1.08X10^5$	0.93
		HM	74.8	$3.61\ x10^8$	$8.31X10^1$	$7.17X10^4$	$1.03X10^5$	0.92
2	45-267	CR	22.1	1.55 x10	$2.44X10^2$	$1.85X10^4$	$1.23X10^5$	0.90
		HM	18.3	$6.81\ x10^1$	$2.51X10^2$	$1.48X10^4$	$1.23X10^5$	0.93
3	47-145	CR	23.2	$1.11\ x10^5$	$1.50X10^2$	$2.01X10^4$	$7.55X10^4$	0.92
		HM	28.3	$8.29\ x10^1$	$2.10X10^2$	$2.52X10^4$	$1.03X10^5$	0.92
4	45-220	CR	66.4	$4.33\ x10^6$	$1.20X10^2$	$6.30X10^4$	$1.12X10^5$	0.94
		HM	54.2	$6.68X10^3$	$1.00X10^1$	$5.60X10^4$	$1.04X10^4$	0.93

Table 8: Energy values obtained in docking calculations of ligand (**HL**) with receptor breast cancer mutant 3hb5 and prostate cancer mutant 2q7k.

Mutant	Est. Free Energy of Binding kCal.mol^{-1}	Est. Inhibition Constant, K_i uM	vdW + Hbond + desolv Energy kCal.mol^{-1}	Electrostatic Energy kCal.mol^{-1}	Total Intermolec. Energy kCal.mol^{-1}	Interact. Surface
3hb5	-6.61	14.24	-8.86	-0.13	-8.99	901.53
2q7k	-0.90	21.92	-3.04	-0.12	-3.16	583.95

Table 9. Decomposition energy of the ligand (**HL**) with breast cancer 3hb5 and prostate cancer 2q7k.

Mutant	Hydrogen bonds	Hydrophobic		Other
3hb5	GLY92 (-0.68) SER12 (-0.55)	PHE192 (-1.43) ALA91 (-0.90) ILE14 (-0.83) VAL188 (-0.32) VAL113 (-0.20)		ARG37 (-0.97) THR140 (-0.34) TYR155 (-0.25)
2q7k	ARG752 (-0.60) GLN711 (0.18)	PHE764 (-1.34) PHE876 (-1.08) LEU701 (-0.67) PHE891 (-0.65) MET749 (-0.40)	MET745 (-0.35) LEU873 (-0.31) MET787 (-0.25) LEU707 (0.96) LEU880 (1.20)	VAL746 (-0.64) MET780 (0.16) ASN705 (0.82) THR877 (1.33)

Table 10. Cytotoxicity of ligand (**HL**) and its metal complexes (**1-4**) against human breast cancer (MCV-7) cell lines.

Conc. µg/ml	Cell viability %				
	HL	**1**	**2**	**3**	**4**
0.00	100.00	100.00	100.00	100.00	100.00
0.10	94.79	88.74	84.58	98.96	96.29
1.00	90.81	74.57	81.74	94.32	95.35
10.00	83.89	60.65	80.56	92.16	84.73
100.00	12.56	32.90	44.45	15.83	9.20
1000.00	10.42	2.47	7.37	11.14	5.78

Table 11. IC_{50} (µg/ml) values of ligand (**HL**) and its metal complexes (**1-4**) against human breast cancer cell.

IC_{50}	**HL**	**1**	**2**	**3**	**4**
µg/ml	30.00	31.00	77.60	39.00	29.00

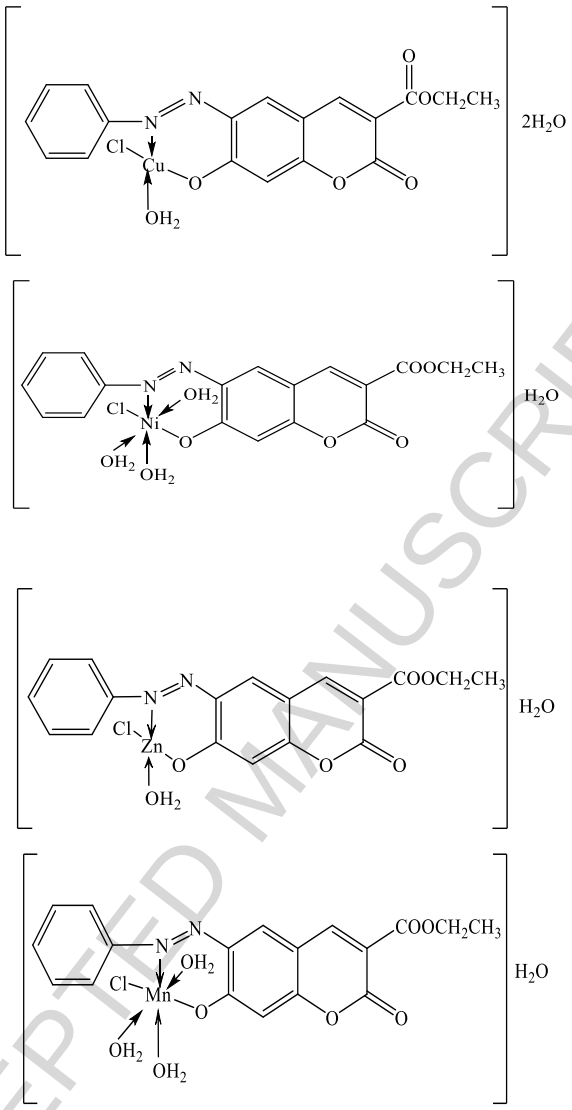

Fig. 1. The proposed structures of Cu(II), Ni(II), Zn(II) and Mn(II) complexes.

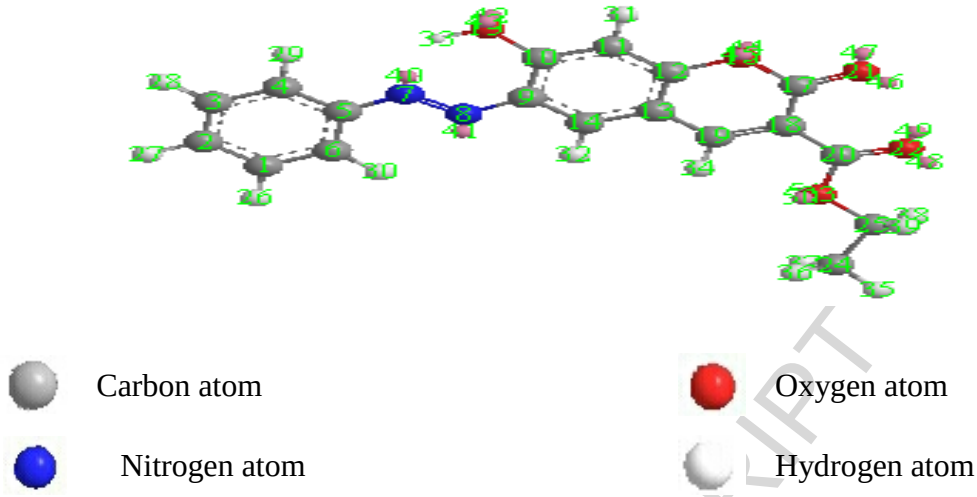

Fig. 2. The calculated molecular structures of the investigated ligand (HL).

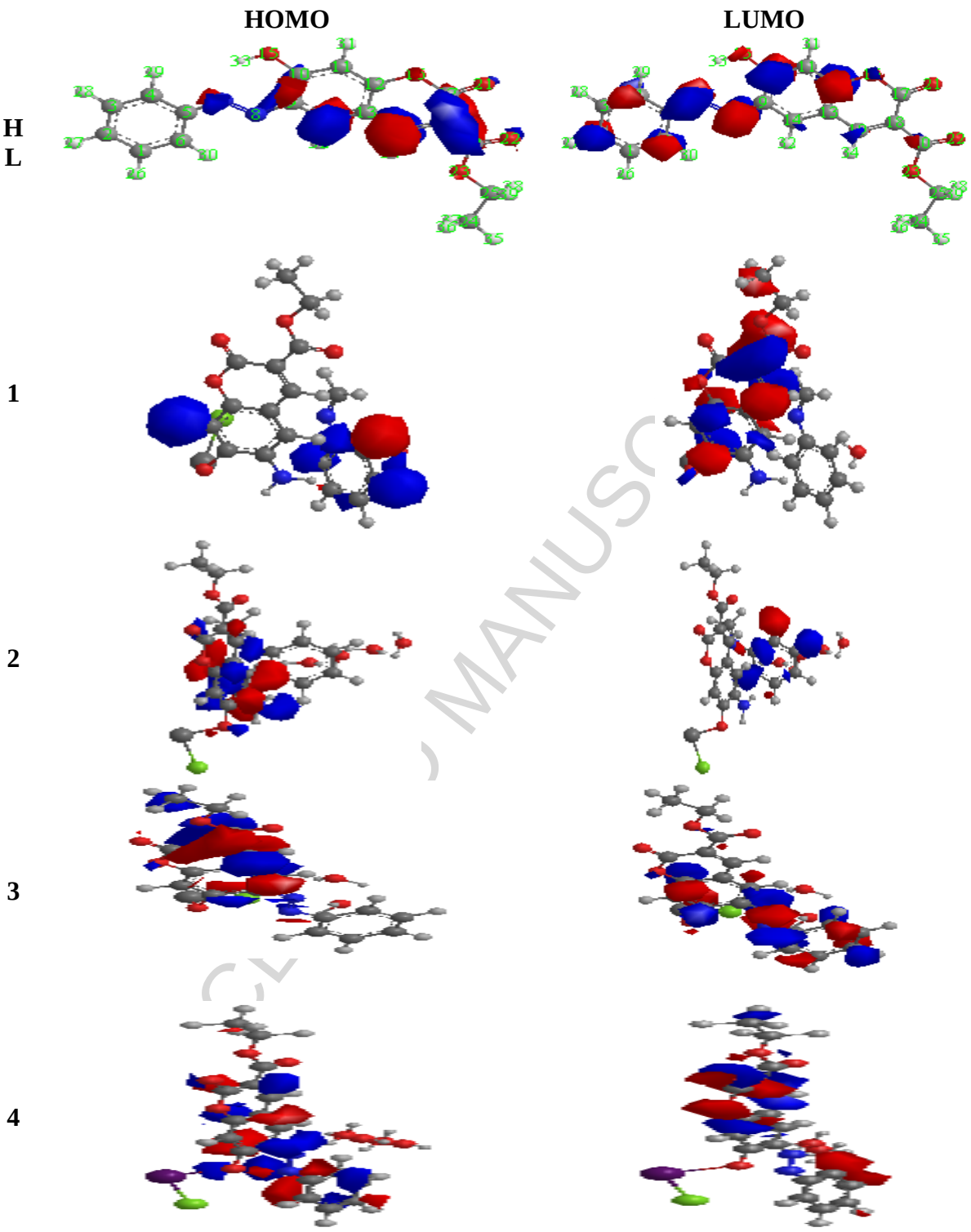

Fig. 3. The Highest Occupied Molecular Orbital (HOMO) and the Lowest Unoccupied Molecular Orbital (LUMO) of the investigated ligand (**HL**) and its metal complexes (**1-4**).

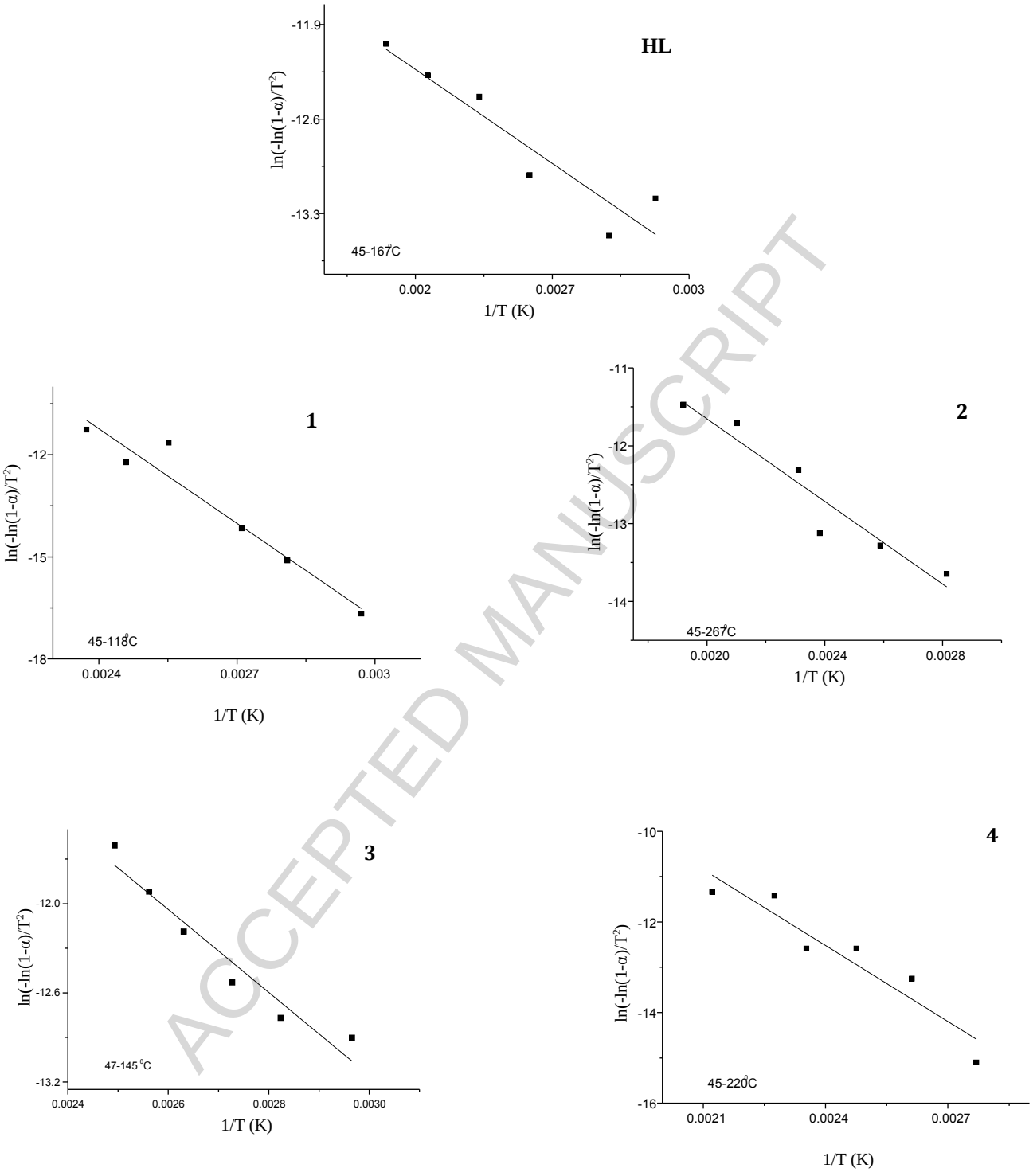

Fig. 4. Coats–Redfern (CR) of the ligand (**HL**) and its metal complexes (**1-4**).

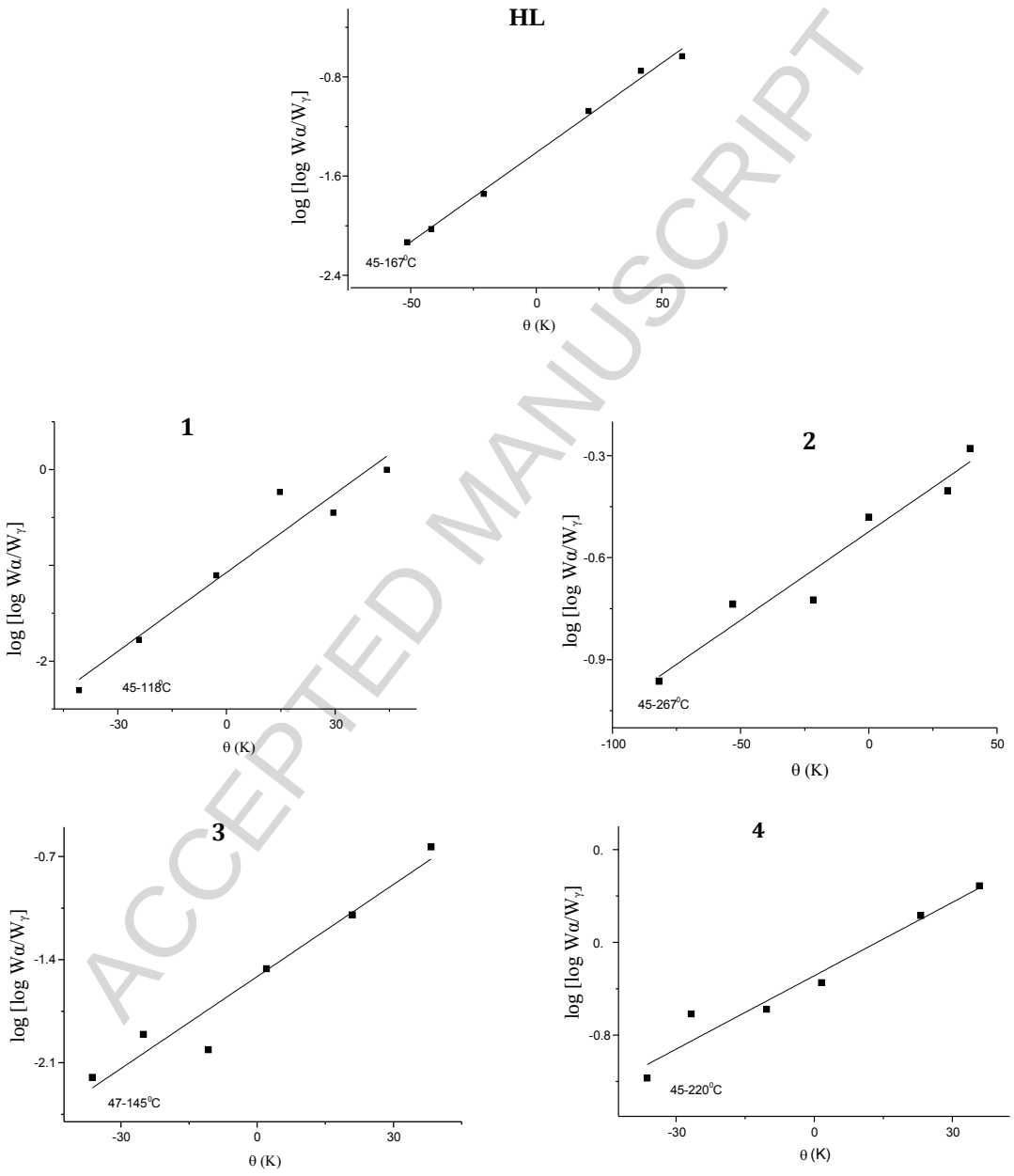

Fig. 5. Horowitz-Metzger (HM) of the ligand (**HL**) and its metal complexes (**1-4**).

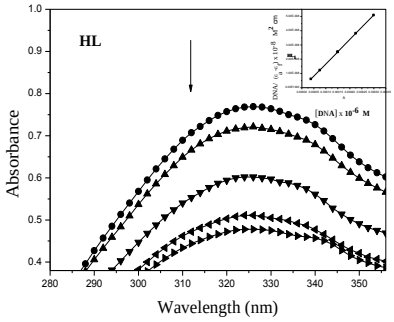

Fig. 6. Absorption spectra of ligand (**HL)** in buffer pH 7.2 at 25 ^{o}C in the presence of increasing amount of CT-DNA. Arrows indicate the changes in absorbance upon increasing the CT-DNA concentration. Inset: plot of [DNA]/($\varepsilon_a - \varepsilon_f$) × 10^{-8} M^2.cm *vs.* [DNA] × 10^{-6} M for titration of DNA with ligand (**HL**).

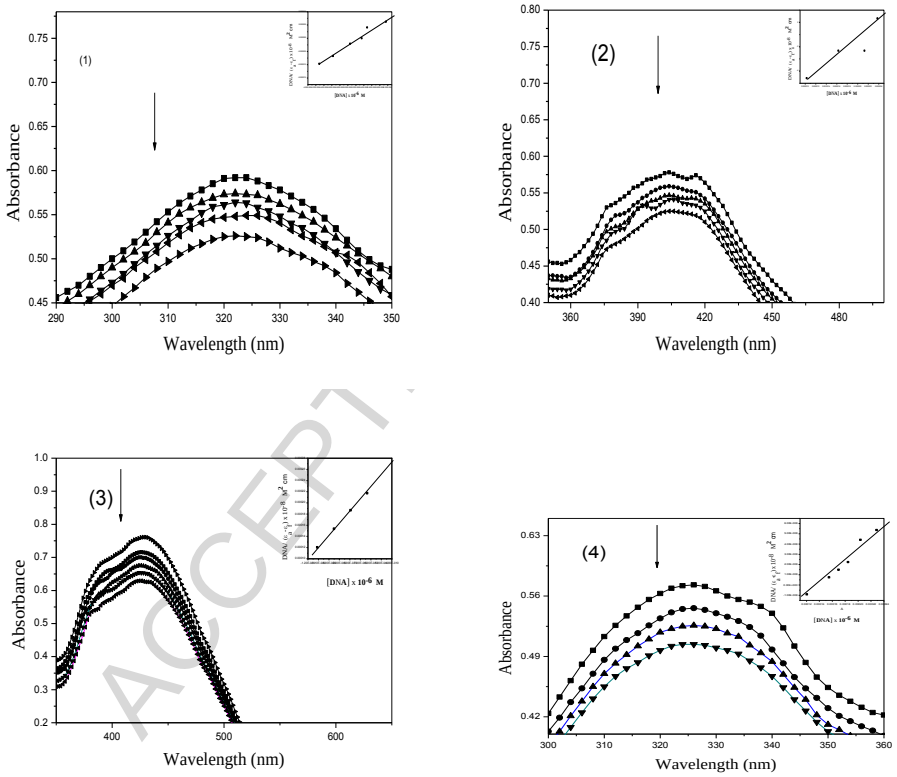

Fig. 7. Absorption spectra of metal complexes (**1-4**) in buffer pH 7.2 at 25 ^{o}C in the presence of increasing amount of CT-DNA. Arrows indicate the changes in absorbance upon increasing the CT-DNA concentration. Inset: plot of [DNA]/($\varepsilon_a - \varepsilon_f$) × 10^{-8} M^2.cm *vs.* [DNA] × 10^{-6} M for titration of CT-DNA with complexes (**1-4**).

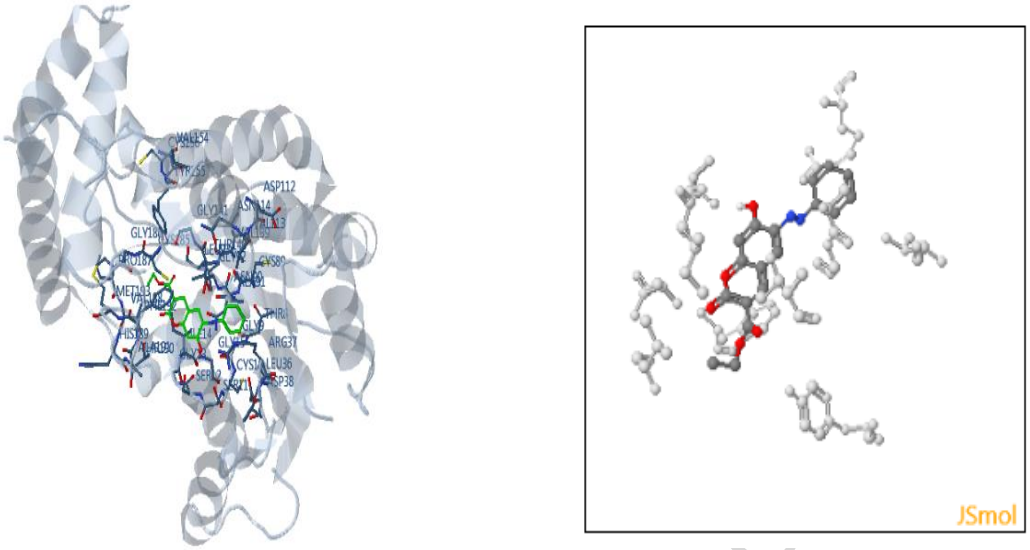

A B

Fig. 8. The ligand (**HL**) (green in (A) and blue in (B) in interaction with receptor breast cancer mutant 3hb5. (For interpretation of the references to color in this figure legend, the reader is referred to the web version of this article).

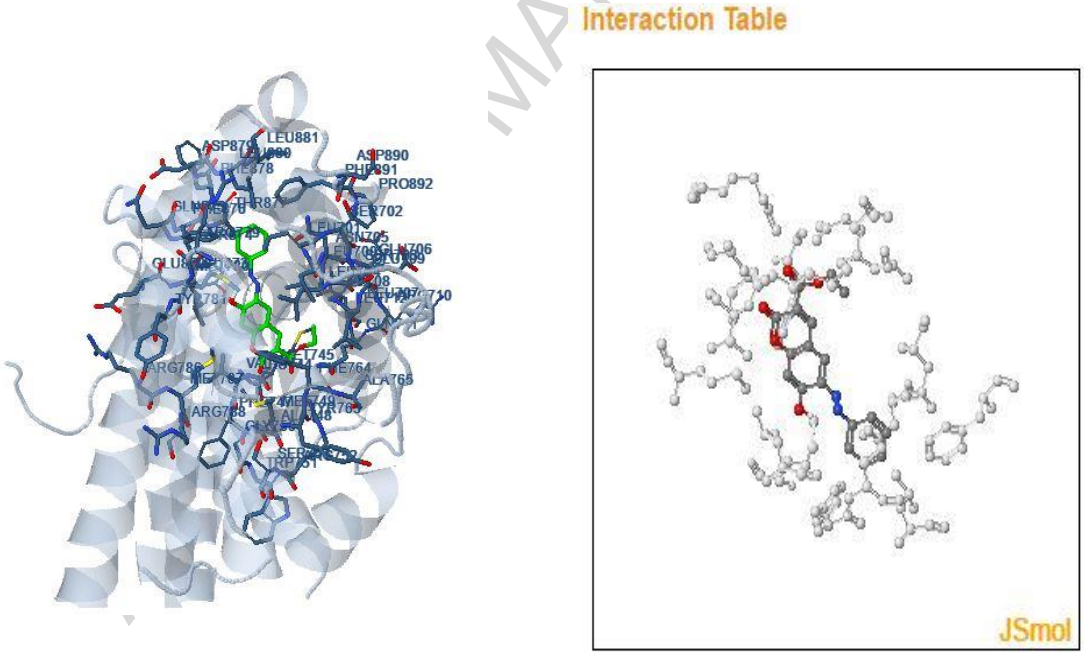

C D

Fig. 9. The ligand (**HL**) (green in (C) and blue in (D) in interaction with receptor prostate cancer mutant 2q7k. (For interpretation of the references to color in this figure legend, the reader is referred to the web version of this article).

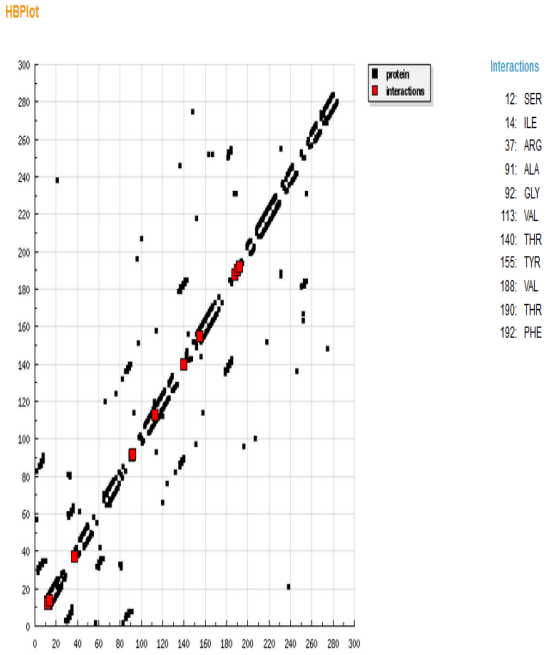

Fig. 10. HB plot of interaction between the ligand (**HL**) and receptor breast cancer mutant 3hb5.

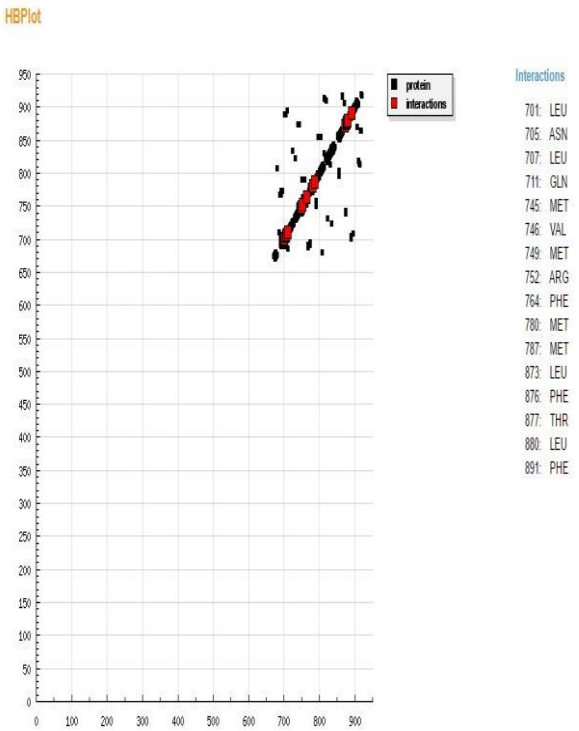

Fig. 11. HB plot of interaction between the ligand (**HL**) and receptor prostate cancer mutant 2q7k.

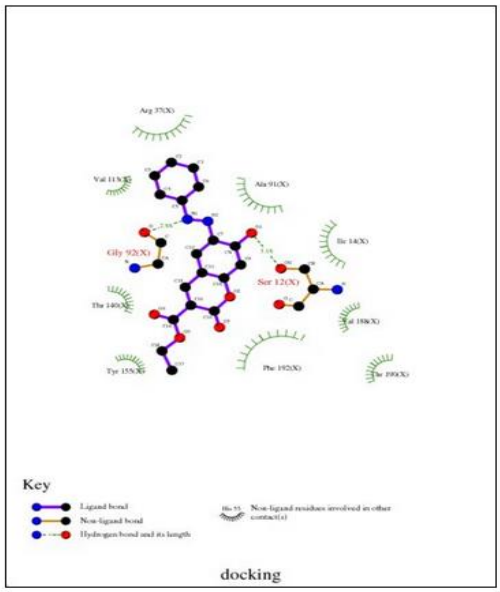

Fig. 12. 2D plot of interaction between the ligand (**HL**) and receptor breast cancer.

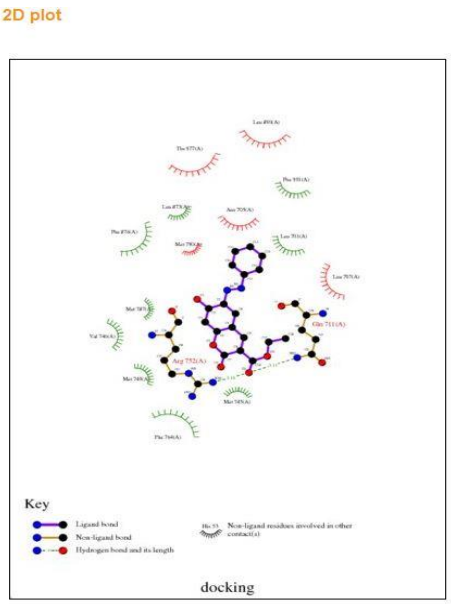

Fig. 13. 2D plot of interaction between the ligand (**HL**) and receptor prostate cancer.

Highlights

- Azo coumarin ligand and their complexes.
- Molecular structure and molecular docking.
- CT DNA binding by absorption spectra.
- Antitumor activity.